

# Calibration of a $\Delta E$ -E telescope based on $\text{CeBr}_3$ scintillator for secondary charged particles measurements in hadron therapy

---

L. Gesson<sup>a,b</sup> J. Gross<sup>1a</sup> C. Mozzi<sup>1a</sup> C. Reibel<sup>a</sup> Ch. Finck<sup>a</sup> S. Higuieret<sup>a</sup> T.D. Lê<sup>a</sup>  
E. Traykov<sup>a</sup> J.C. Thomas<sup>d</sup> N. Arbor<sup>a</sup> M. Pullia<sup>c</sup> G. Harmant<sup>a</sup> M. Vanstalle<sup>a</sup>

<sup>1</sup>Both authors contributed equally

<sup>a</sup>Universite de Strasbourg, CNRS, IPHC UMR 7178, Strasbourg, 67000, France

<sup>b</sup>GSI Helmholtzzentrum fur Schwerionenforschung GmbH, Darmstadt, 64291, Germany

<sup>c</sup>CNAO Centro Nazionale di Adroterapia Oncologica, Pavia, 27100, Italy

<sup>d</sup>GANIL Grand Accélérateur National d'Ions Lourds, CEA-DRF, CNRS, Caen, 14000, France

E-mail: [levana.gesson@iphc.cnrs.fr](mailto:levana.gesson@iphc.cnrs.fr)

**ABSTRACT:** Hadrontherapy is a promising cancer treatment method that offers better dose conformity and reduces damage to healthy tissues compared to conventional radiotherapy. However, one major challenge remaining is the precise characterization of secondary particles generated by nuclear interactions of the primary beam with tissues. Current data on secondary charged particles, such as protons and light ions, remain insufficient, particularly in the clinically relevant energy ranges. This lack of experimental data introduces uncertainties in treatment planning softwares and Monte Carlo calculations, thus compromising the accuracy of dose delivery to the patients.

This work consists in the characterization of secondary charged particles generated in hadrontherapy using a  $\Delta E$ -E telescope comprising a  $\text{CeBr}_3$  crystal scintillator and a plastic scintillator. The calibration and response of this telescope to ions commonly used in clinical settings is presented in this work, highlighting adherence to Birks' law for accurate energy measurements.

This study is the first to optimize a  $\Delta E$ -E telescope combining  $\text{CeBr}_3$  and plastic scintillators specifically for secondary particle detection in hadrontherapy. This represents an important step in the exploitation of the system for nuclear data acquisition, as it enables both the measurement of energy and the discrimination of secondary particles. The objective is to develop a system compatible with clinical use, allowing for the most precise possible comparison with treatment planning software calculations.

**KEYWORDS:** Instrumentation for particle-beam therapy, Scintillators,  $dE/dx$  detectors, Heavy-ion detectors, Ion identification systems, Instrumentation for hadron therapy, Instrumentation for heavy-ion therapy

ARXIV EPRINT: [1234.56789](https://arxiv.org/abs/1234.56789)

---

## Contents

<b>1</b>	<b>Introduction</b>	<b>1</b>
<b>2</b>	<b>Material and Methods</b>	<b>2</b>
2.1	Detectors description	2
2.2	Experimental setup	3
2.3	Analysis of the data	4
2.4	Monte Carlo simulations	7
<b>3</b>	<b>Results</b>	<b>8</b>
3.1	Response of the plastic scintillator	8
3.2	Response of the CeBr <sub>3</sub> to ions	9
3.3	Telescope ions identification	13
3.4	Time performance	14
<b>4</b>	<b>Discussion</b>	<b>15</b>
<b>5</b>	<b>Conclusion</b>	<b>16</b>

---

## 1 Introduction

Particle therapy, including proton and heavy-ion therapy, has demonstrated significant advantages over conventional X-ray radiotherapy by providing highly conformal dose distributions to the tumor while better sparing surrounding healthy tissues [13] [22].

However, the interactions between the primary particle beam and human tissue lead to nuclear fragmentation, producing secondary particles such as lighter ions, neutrons, and gamma rays. These secondary particles can cause various types of damage, including ionization, excitation, and fragmentation of molecular bonds. This damage can affect cellular functions and lead to biological responses that can contribute to undesired dose in healthy organs and tissues [29] [9].

Accurate dose calculations for particle therapy are critically dependent on high-performance algorithms that model complex physical and biological processes, often using data generated through Monte Carlo simulations [28] [3]. However, there is currently a lack of experimental data regarding nuclear reactions in particle therapy, which can introduce inaccuracies in dose calculations [19][25].

The CLINM (Cross-Sections of Light Ions and Neutron Measurements) project, addresses this gap by focusing on the precise characterization of secondary particles produced during ion fragmentation in tissues, in order to compare with Monte Carlo simulations and improve their accuracy.

One key point of the CLINM project is to measure the yields, charges, and energies of the fragments produced under conditions that replicate clinical experimental settings. In this work, the focus will be on the charged secondary particles. To achieve this, a  $\Delta E$ -E telescope detection system has been developed. This technique leverages the principles of energy loss and remaining energy to discriminate different particle charges. The thinner detector in the telescope, a plastic scintillator, measures the energy loss ( $\Delta E$ ) of charged particles as they pass through, while a  $\text{CeBr}_3$  crystal scintillator measures the remaining energy (E) of the particle.

Before employing this system for nuclear data acquisition on the production of secondary charged particles in hadrontherapy, it is essential to characterize it and assess its measurement performance. This includes energy calibration, energy resolution, ion discrimination capability in the  $\Delta E$ -E mode, and time resolution for correlation studies or even time-of-flight measurements.

The presented research aims to characterize the response of the  $\Delta E$ -E telescope to ions used in clinical therapy by analyzing their energy deposition patterns in the two components. Unlike previous studies, this work employs a  $\text{CeBr}_3$  scintillator, a choice for heavy-ion detection in hadrontherapy applications, owing to its unique properties of high light yield, fast timing, and low intrinsic background radiation. This marks a significant improvement over traditional scintillators (e.g., NaI or  $\text{LaBr}_3$ ) that suffer from limitations such as internal radioactivity or saturation at high energies.

In this study, the primary beams simulate the clinical energy ranges used in therapy, but the focus remains on the secondary charged particles generated during beam interactions with materials mimicking patient tissues (e.g., PMMA). This telescope is designed to measure energy deposition patterns of these secondary charged particles, which include protons, light ions (e.g., deuterons, alpha particles), and heavier fragments generated by nuclear fragmentation processes, with energies ranging from a few MeV up to 200 MeV/u.

## 2 Material and Methods

### 2.1 Detectors description

The  $\Delta E$ -E telescope is composed of two scintillating detectors: a thin plastic scintillator ( $\Delta E$ ) and a thick crystal scintillator of  $\text{CeBr}_3$  (E), long enough to stop  $^{12}\text{C}$  up to 200 MeV/u (Figure 2).

The  $\text{CeBr}_3$  detector is a cylindrical 2×2 inches crystal scintillator, from Advatech UK Ltd [1], coupled to a R6231-100 Hamamatsu photomultiplier (PMT). An entrance window in front of the crystal inside the  $\text{CeBr}_3$  is made of 400  $\mu\text{m}$  of aluminum and 1 mm of polytetrafluoroethylene (PTFE), used as a reflector. The  $\text{CeBr}_3$  detector has a short decay time of 19 ns, a high light yield of 60,000 Photons/MeV, an energy resolution of 3.8 keV at 662 keV for X-ray and gamma-ray, and an inherent low background radiation of 0.004 Bq/cm<sup>3</sup>.

The  $\text{CeBr}_3$  crystal scintillator was chosen for its capacities to detect not only charged particles but also gamma rays and neutrons, aligning well with the general context of CLINM. Unlike some alternatives like  $\text{LaBr}_3$ ,  $\text{CeBr}_3$  does not exhibit internal radioactivity, which minimizes background noise and false coincidences, thus enhancing the precision of radiation detection.

Concerning the voltage applied on the R6231-100 Hamamatsu PMT coupled to the  $\text{CeBr}_3$ , the constructor recommended value is + 1200 V. However, the voltages applied were of + 400 V and

+ 350 V, in order to detect the high-energy protons and  $^{12}\text{C}$  without reaching the PMT saturation, following recommendations from [21][24].

The plastic scintillator, from Eljen Technology (EJ-228), is a square of  $6\times 6\times 0.2\text{ cm}^3$ , put in front of the  $\text{CeBr}_3$ . The plastic detector has a short decay time of 1.4 ns, and a light yield of 10,200 Photons/MeV. This plastic scintillator is designed to deliver high performance in terms of timing resolution and light output, making it ideal for our specific needs.

Two different photomultipliers (PMT) from Hamamatsu, R7057 and XP3990, were tested, coupled to the plastic scintillator, supplied with -1100V and -1200V high-voltage respectively, in order to optimize the settings, i.e. minimize saturation while maximizing resolution.

Both detectors signals were acquired in coincidence by a WaveCatcher digitizer module, developed by the LAL laboratory (Paris, France) [6]. The sampling frequency was set to be 3.2 GHz on the DAQ. Figure 1 illustrates digitized signals obtained from the plastic scintillator and  $\text{CeBr}_3$  crystal when irradiated with 200 MeV/u  $^{12}\text{C}$  ions. As expected, the pulse duration and the rising time of the plastic scintillator ( $\sim 1.4\text{ ns}$ ) are shorter than the ones from the  $\text{CeBr}_3$  ( $\sim 19\text{ ns}$ ), in accordance with intrinsic properties of both scintillators. A gate of 80 ns was applied for the detector's coincidence detection.

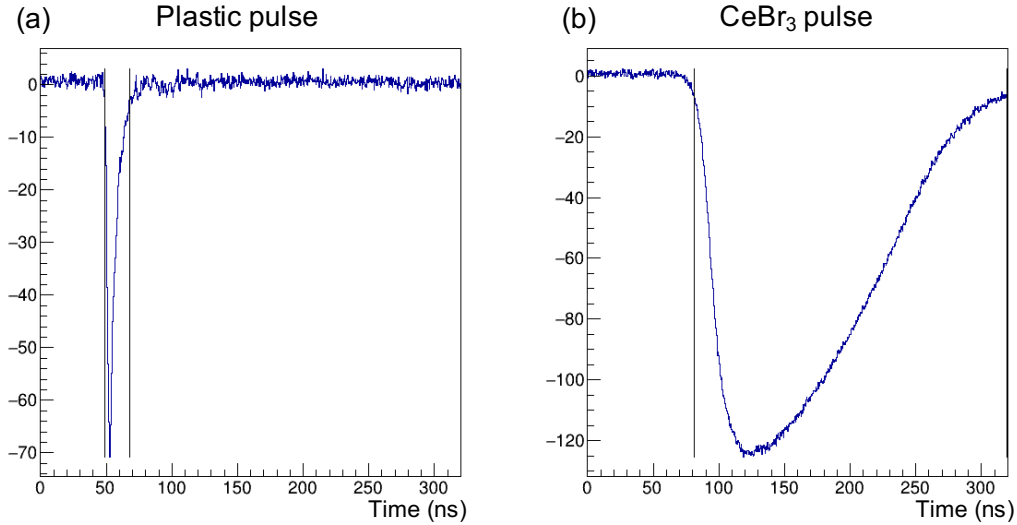


**Figure 1.** Pulse shape of the signal obtained with the plastic scintillator with -1200V applied (a) and  $\text{CeBr}_3$  crystal with +350V applied (b) irradiated with 200 MeV/u  $^{12}\text{C}$ .

## 2.2 Experimental setup

Experiments were carried out in different facilities providing ions of various types and energies: Cyréc cyclotron at IPHC (Strasbourg, France) [12], producing protons beam of 25MeV, which can be attenuated by an aluminium wheel to lower energies ; CAL (Centre Antoine Lacassagne, Nice, France) protontherapy center [17], specializes in proton therapy treatments for cancer, providing

a proton beam of 62 MeV ; cave M of GSI (Darmstadt, Germany), the heavy ion accelerator facility SIS-18 [14], using PMMA thickness variations to modulate carbon beam energies ; CNAO hadrontherapy center (Pavia, Italy) [23], which offers advanced hadron therapy treatments using carbon ions and protons ; the LISE spectrometer [4] of the GANIL facility (Caen, France), producing lithium ion beam of 63.6 MeV/u and carbon ion beam of 75.4 MeV/u, which can be degraded by PMMA wheel to lower energies. The characteristics of the beams which were used are summarised in Table 1. The different experimental setups for each facilities are presented on Figure 2.

Facility	Ion type	Energy range
Cyrcé	$^1\text{H}$	16 - 25 MeV
CAL	$^1\text{H}$	61 MeV
GSI	$^{12}\text{C}$	120 - 180 MeV/u
CNAO	$^1\text{H}$	80 - 180 MeV
CNAO	$^{12}\text{C}$	120 - 200 MeV/u
GANIL	$^{12}\text{C}$	30 - 75 MeV/u
GANIL	$^8\text{Li}$	45 - 64 MeV/u

**Table 1.** Beam types and energies that were used for the calibration of the  $\text{CeBr}_3$  and plastic scintillators.

At Cyrcé, aluminum attenuators from 0.147 mm to 1.424 mm were used to degrade the beam energy from 25 MeV down to 16 MeV, while at GSI, three different PMMA thicknesses were used in order to achieve carbon beam energy ranges of 120 MeV/u, 160 MeV/u and 180 MeV/u. At CAL and CNAO, the energy of the beam was not attenuated. Only one energy of 61 MeV/u was used at CAL, while several energies of  $^{12}\text{C}$  and protons were used at CNAO, from 120 MeV/u to 200 MeV/u. In the experimental setup at GSI, a plastic scintillator of 1 mm was placed in front of the beam for another experiment which was carried out at the same beam time. At GANIL, to attenuate the energy of the beam, a specific experimental setup with a wheel was developed and build, with thirty different PMMA thicknesses in order to achieve carbon beams from 30 MeV/u to 64 MeV/u and lithium beams from 45 MeV/u to 75 MeV/u. The plastic detector was replaced with two silicon detectors, each 0.2 mm thick, for an additional test phase aimed at improving resolution for the CLINM project.

### 2.3 Analysis of the data

The used analysis software package was an extension of the QAPIVI software tool [11], called STIVI (Software for Tracking of Ions and Vertex Imaging). The baseline refers to the initial portion of the waveform where no significant signal is expected, representing the underlying noise level of the system. To establish the baseline of the waveforms, the projection of the first 10 bins in time was employed on the pulse shape. Subsequently, the mean value and dispersion, indicative of the noise level, were computed for accurate characterization.

The determination of the signal's rise and fall involved setting thresholds relative to the baseline, typically defined as the baseline minus 10 times the noise level.

The integration of the signal giving the charge was then performed within the determined range, while the amplitude of the signal was identified as its maximum value. The baseline of

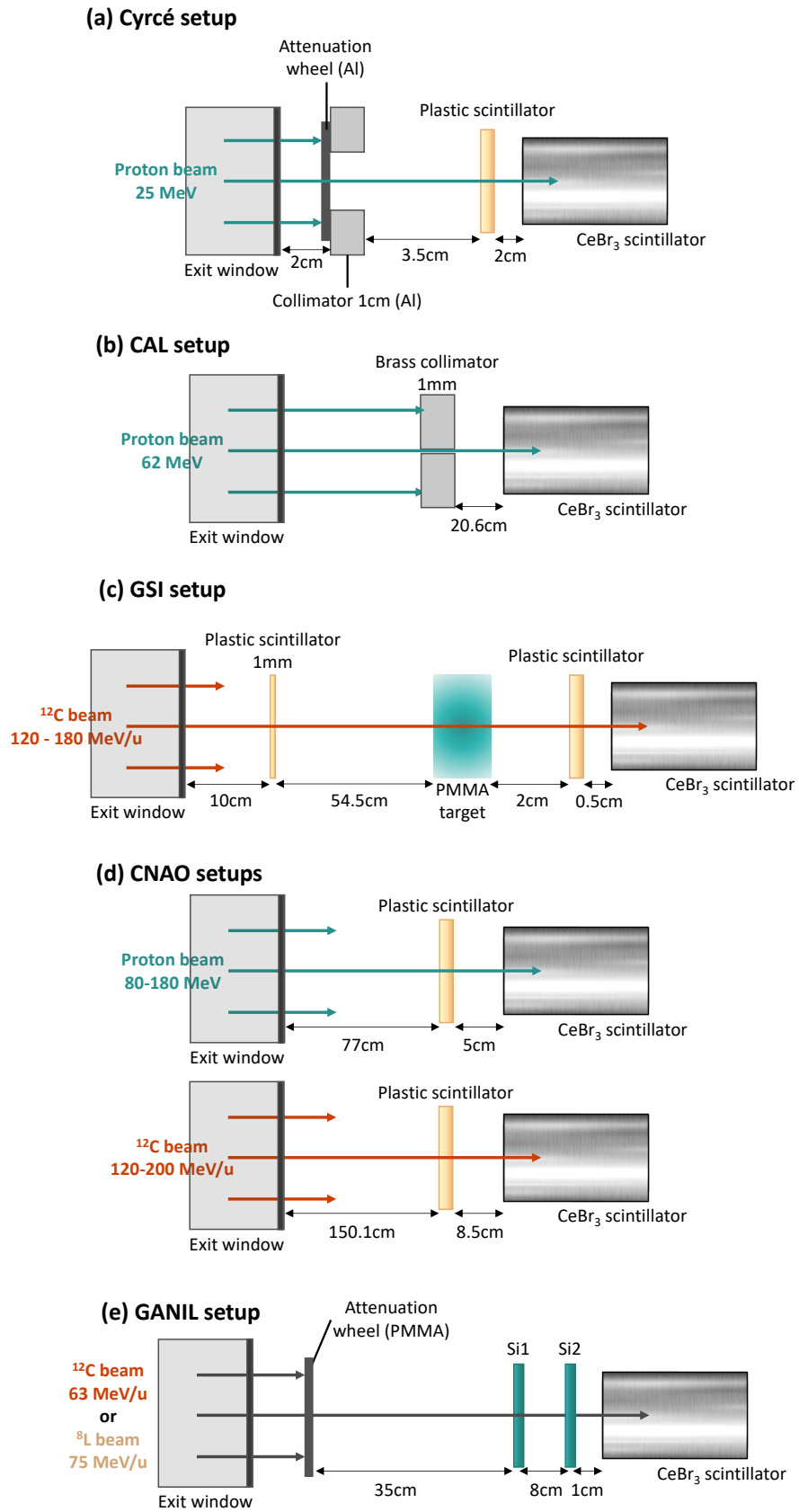


**Figure 2.** Schemes of the experimental setups used at Cyrcé (a), CAL (b), GSI (c), CNAO (d) and GANIL (e) facilities.

the waveforms was subtracted to the signal, to isolate the signal from the background noise. The distributions of the amplitudes of the Waveforms (in mV) were fitted with Gaussian functions, in order to extract the mean amplitude value and its corresponding standard deviation.

The analysis of the signal characteristics, including rise and fall times, amplitude, and charge integration, is crucial for accurately interpreting the detector response. A key aspect of this calibration process is accounting for the specific scintillation response of the detector to different particle types and their energy deposition patterns.

Initially formulated by J.B. Birk (1951), Birk's law describes the non-linear response of scintillators to ionizing radiation, taking into accounts the scintillation quenching, a phenomenon wherein scintillator efficiency decreases as the local ionization density along the particle track increases. The classical formulation of Birk's law [5] is as follows:

$$\frac{dL}{dx} = \frac{S \cdot \frac{dE}{dx}}{1 + k_B \cdot \frac{dE}{dx}}$$

where  $\frac{dL}{dx}$  is the light output per unit length,  $\frac{dE}{dx}$  is the energy deposited per unit length by the particle,  $S$  is a proportionality constant that translates the energy deposited into light output (which can be attributed to scintillation efficiency),  $k_B$  is Birk's constant, representing the scintillator-specific quenching parameter, with typical values ranging from  $10^{-2}$  to  $10^{-3}$  cm/MeV for common scintillators [18].

In practical applications, the differential energy loss  $\frac{dE}{dx}$  is often unknown. Instead, the total energy deposited is typically measured,  $E$ , alongside the resulting pulse amplitude from the scintillator. To address this, Birk's law was adapted to use total deposited energy rather than the differential loss. This modified approach adjusts the original constants, replacing  $S$  and  $K_B$  with  $S'$  and  $k'_B$  to reflect total energy considerations, leading to the adapted formulation:

$$A = \frac{S' \cdot E + A_0}{1 + k'_B \cdot E}$$

where  $A$  is the amplitude of the light signal measured (in mV),  $E$  is the total energy deposited (in MeV),  $S'$  is a conversion factor between the deposited energy and the amplitude,  $k'_B$  is a modified quenching parameter adapted to total energy (in  $\text{MeV}^{-1}$ ),  $A_0$  represents a pedestal or baseline signal (in mV) accounting for background noise or residual detector response.

The adjusted conversion factor  $S'$  serves as a proportionality factor to convert the deposited energy  $E$  into the expected amplitude  $A$ , reflecting both light yield efficiency and the detector's response, with typical values ranging from  $\sim 10^{-2}$  to  $10^0$  mV.MeV $^{-1}$  [18][5][8]. Unlike  $S$ , which relates to differential energy loss,  $S'$  is calibrated to reflect the detector's pulse response to total energy deposition. The adjusted quenching parameter  $k'_B$  represents saturation effects related to total energy deposited, with values typically ranging from  $10^{-2}$  to  $10^{-3}$  MeV $^{-1}$  for inorganic scintillators [10] and from  $10^{-3}$  to  $10^{-4}$  MeV $^{-1}$  for organic or plastic scintillators [7], aligning with Birk's quenching model. The pedestal  $A_0$  accounts for baseline signal amplitude from residual detector response, typically in the low mV range. The adapted Birk's law maintains the quenching

effect via  $k'_B$  while incorporating linear responses at low energy deposition through  $S'$ .

For the next sections, the function will be used as follows, with  $p_0$ ,  $p_1$  and  $p_2$  the variable parameters, and, for simplicity,  $S'$  and  $k'_B$  will be referred to as  $S$  and  $k_B$ , respectively:

$$A = \frac{p_0 * E + p_1}{1 + p_2 * E} \quad (2.1)$$

These three parameters are dependent on the geometry of the scintillators and the high voltage applied to the PMT. Thus, they were considered as free parameters in the fit of the detector response to ions, and represent the calibration parameters values of our detectors.

Additionally, the optimization of the applied voltage was investigated to determine the best operating conditions for different ion species, ensuring both signal quality and accurate particle identification.

Beyond energy calibration, another crucial aspect of the system's characterization is its suitability for time-of-flight (TOF) measurements. The ability to resolve detection times with high precision is fundamental for identifying secondary particles and reconstructing their kinematics. Therefore, the time resolution of the telescope was assessed by quantifying detection time differences and analyzing the distribution's standard deviation, providing key insights into the temporal capabilities of the system.

## 2.4 Monte Carlo simulations

The Monte Carlo code `GEANT4 10.07` [3] with the `INCL++` physic list [2] was used to evaluate the deposited energy in the plastic scintillator, and the energy of the ions reaching the  $\text{CeBr}_3$  crystal, after its entrance window. While it is not necessary to take into account the thickness of this entrance window for  $\gamma$ -rays detection, it needs to be considered for ions detection, as they will lose a non-negligible amount of energy inside.

Simulations were also used to evaluate the energy straggling and beam scattering. Indeed, contrary to gamma-rays measurements, where the standard deviation around the mean energy value corresponds to the detector resolution at the considered energy, charged particles encounter important straggling in the different materials they cross, manifesting as a spread in the energy loss distribution, contributing to the observed broadening of the energy spectrum in detectors. Alongside, beam scattering, arising from multiple Coulomb scattering events experienced by charged particles, induces deviations from their initial trajectories, thereby influencing the spatial distribution of energy deposition.

To rigorously quantify the intrinsic energy resolution of each detector, it is imperative to disentangle the contributions from energy straggling and beam scattering from the overall detector resolution. This requires subtracting the standard deviation derived from the Monte Carlo simulations,  $\sigma_{G4}$ , from the standard deviation obtained from the experimental data calibration,  $\sigma_{det}$ , as per the equation [29][26]:

$$\sigma_E = \sqrt{\sigma_{det}^2 - \sigma_{G4}^2} \quad (2.2)$$

where  $\sigma_{det}$  corresponds to the standard deviation of the energy distribution obtained after calibration of the raw data distributions, and  $\sigma_{G4}$  is the standard deviation of the energy distribution



predicted by Geant4. This deviation does not take into account any detector response, and therefore corresponds only to the straggling and beam scattering.

Moreover, the fitting of detector resolution as a function of collected energy using the proposed equation facilitates a comprehensive characterization of the resolution behavior across varying energy depositions. The parameters  $a$  and  $b$  in the equation (3) capture the nuanced dependence of resolution on energy deposition [20][16]:

$$\frac{\sigma_E}{E} = a + \frac{b}{\sqrt{E}} \quad (2.3)$$

with  $a$  and  $b$  being free parameters for the fit.

### 3 Results

#### 3.1 Response of the plastic scintillator

The calibration curve of the plastic scintillator obtained with both protons and  $^{12}\text{C}$  ions is presented on Figure 3 and 4(a) for both photomultipliers. It can be observed in both cases that the Birk's law is verified up to 50 MeV of deposited energy, which corresponds to the energy deposited by  $^{12}\text{C}$  ions of 180 MeV/u (after 30 mm of PMMA) for Figure 3 and by  $^{12}\text{C}$  ions of 120 MeV/u for Figure 4(a). The two calibrations constants cannot be compared with each other because of the two different PMT and voltage applied (-1200V and -1100V).

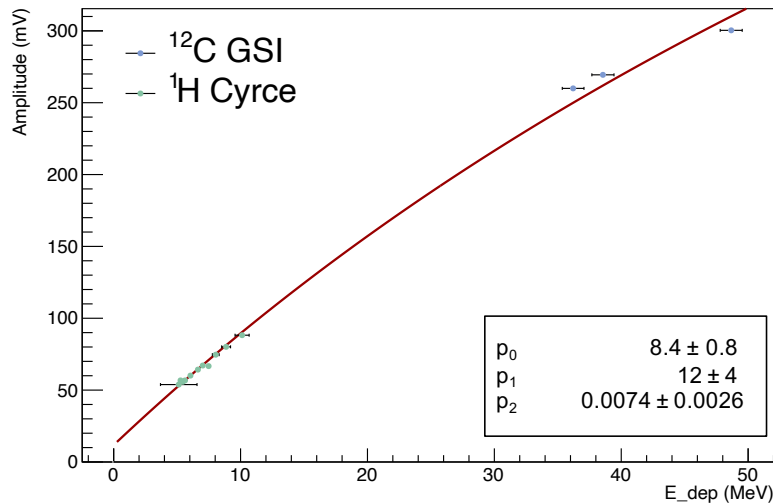


**Figure 3.** Calibration curve of the plastic scintillator with the R7057 PMT at -1100V, with  $^{12}\text{C}$  beams of GSI and  $^1\text{H}$  beams of Cyrce. Energies can be found on Table 1.

The energy resolution of the scintillator with the XP3990 PMT is also shown, as a function of the deposited energy, on Figure 4(b). This analysis integrates considerations of experimental beam

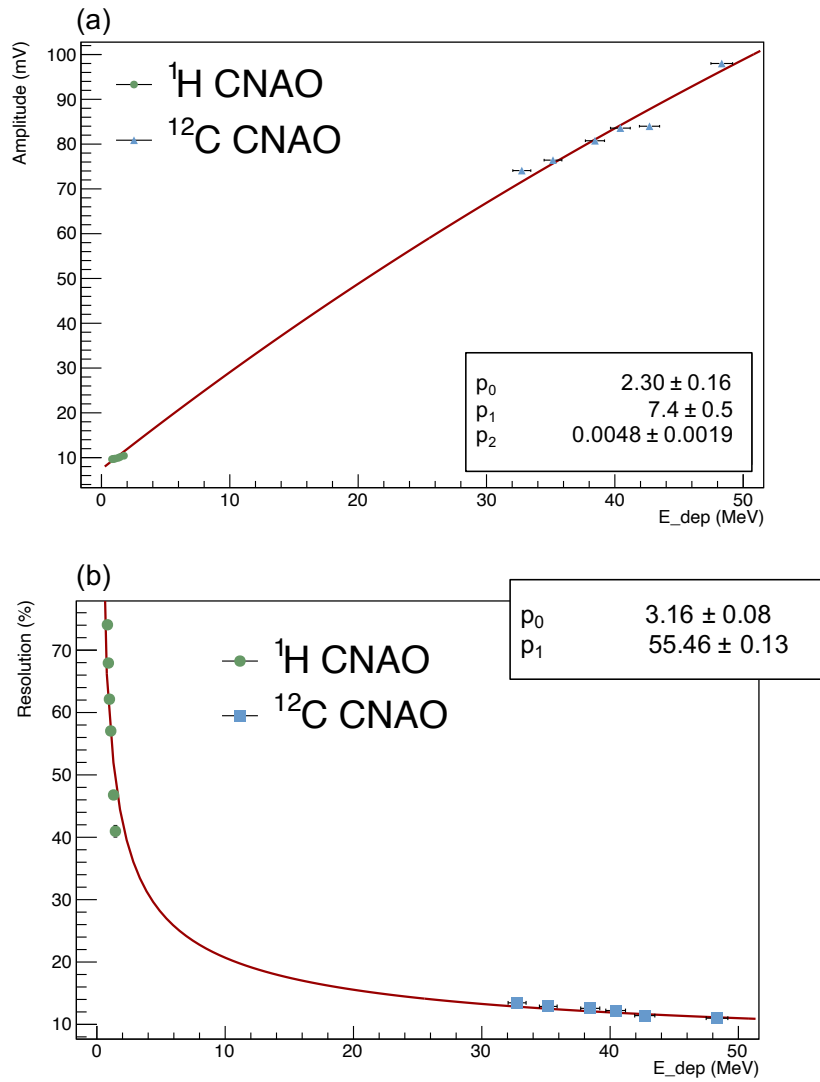


**Figure 4.** Calibration curve of the plastic scintillator with the XP3990 PMT at -1200V (a) and energy resolution as a function of the deposited energy (b), with  $^{12}\text{C}$  and  $^1\text{H}$  beams of CNAO. Energies can be found on Table 1.

straggling effects, which may introduce uncertainties in the measured energy resolution. Indeed, the energy deposited by the ions can exhibit significant variation due to straggling, leading to a spread in the measured energy spectrum. The uncertainty in energy loss can be in the order of several MeV, depending on the thickness and composition of the material. Similarly, scattering can cause angular deviations up to a few degrees, impacting the spatial resolution of the detector.

### 3.2 Response of the $\text{CeBr}_3$ to ions

On Figure 5, the calibration curves of the  $\text{CeBr}_3$  crystal scintillator obtained with both protons and  $^{12}\text{C}$ , with an applied voltage of + 350 V for (a) and obtained with protons,  $^8\text{Li}$  and  $^{12}\text{C}$ , with an

applied voltage of + 400 V for (b), are presented. For each ion type (carbon, lithium and proton), distinct calibration functions are applied and extrapolated to energy ranges not measured. This differentiation is consistent with the findings in [21], where the scintillators' light output showed varying responses based on the isotope. Remarkably, the Birk's constant appears similar in order of magnitude and numerical value for all ions, reflecting a robust consistency in the calibration results. Adherence to Birk's law is observed up to 2350 MeV of deposited energy, corresponding to the energy deposited by  $^{12}\text{C}$  of 200 MeV/u (after traversing 2mm of PMMA). Notably, the plotted points for protons, lithium and carbon ions exhibit a conformal distribution, suggesting a consistent response of the scintillator across different particle types and energies.

All the fit parameters values collected for both plastic and  $\text{CeBr}_3$  and for all the voltage used can be found in Table 2. It can be observed that, depending on the voltage and the photomultiplier gain, distinct Birk's constants are obtained. Nevertheless, it is noteworthy that these discrepancies in Birk's constants across different conditions overlap within the margin of error and fall within the expected range reported in the literature, thereby indicating coherence in the data.

Detector	S	$k_B$ ( $\text{MeV}^{-1}$ )
Plastic -1200V	$8.4 \pm 0.8$	$0.0074 \pm 0.0026$
Plastic -1100V	$2.30 \pm 0.16$	$0.0048 \pm 0.0019$
$\text{CeBr}_3$ +350V (Carbons)	$0.1495 \pm 0.0005$	$0.0008570 \pm 0.0000024$
$\text{CeBr}_3$ +350V (Protons)	$0.3590 \pm 0.0002$	$0.0008638 \pm 0.0000024$
$\text{CeBr}_3$ +400V (Carbons)	$0.67816 \pm 0.00014$	$0.0028710 \pm 0.0000008$
$\text{CeBr}_3$ +400V (Protons)	$1.16617 \pm 0.00029$	$0.003727 \pm 0.000006$
$\text{CeBr}_3$ +400V (Lithiums)	$0.2415 \pm 0.0003$	$0.0007170 \pm 0.0000015$

**Table 2.** Obtained values of free parameters from Birks' law used to fit the detectors calibration curves.

On Figure 6 are presented the energy resolution distribution of the  $\text{CeBr}_3$  obtained with both protons and  $^{12}\text{C}$  for a + 350 V voltage applied for (a), and of the  $\text{CeBr}_3$  obtained with protons,  $^8\text{Li}$  and  $^{12}\text{C}$  for a + 400 V voltage applied for (b). Remarkably, a resolution in the order of maximum 10 MeV is observed for all ion types, underscoring the precision of the crystal in measuring energy depositions.

To validate the calibration of the  $\text{CeBr}_3$  scintillator, experimental data in energy are compared with Geant4 simulations, as depicted in Figure 7. This comparison offers insights into the reliability of the methodology across proton, lithium and carbon ion measurements. Looking into the comparison of deposited energy in  $\text{CeBr}_3$  between Geant4 simulations and calibrated experimental data, using a 120 MeV/u  $^{12}\text{C}$  beam as illustrated in Figure 7(a), the presence of a fragmentation tail is revealed in the experimental data, but less present in the simulation. However, the simulation accurately reproduces the energy peak distribution. Similarly, Figure 7(b) depicts the comparison of  $\text{CeBr}_3$  deposited energy between Geant4 simulations and calibrated experimental data using a 80 MeV  $^1\text{H}$  beam. Here, a discrepancy of less than 5 MeV in the energy peak can be observed. While this deviation is noticeable, it falls within an acceptable range for ensuring the reliability of our measurements. This range, typically defined as  $\pm 5\%$ , accounts for minor variations in experimental conditions and calibration inconsistencies. Specifically, a 5 MeV discrepancy in the context of a 80

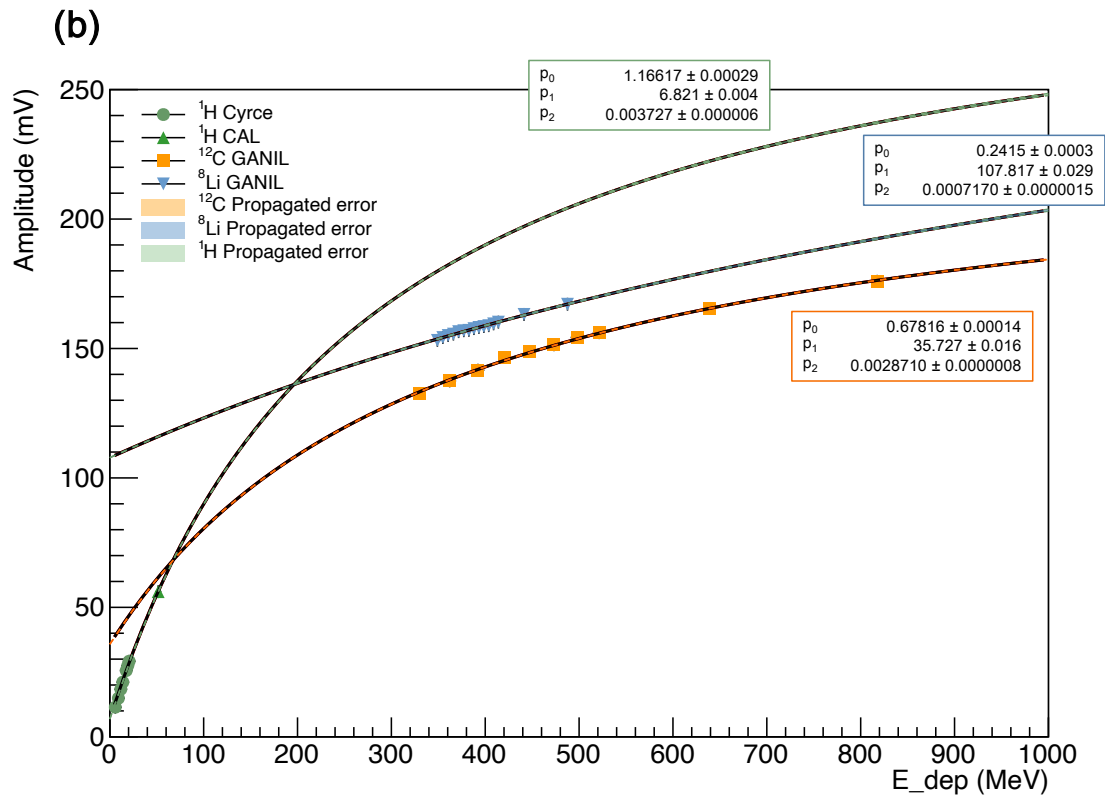
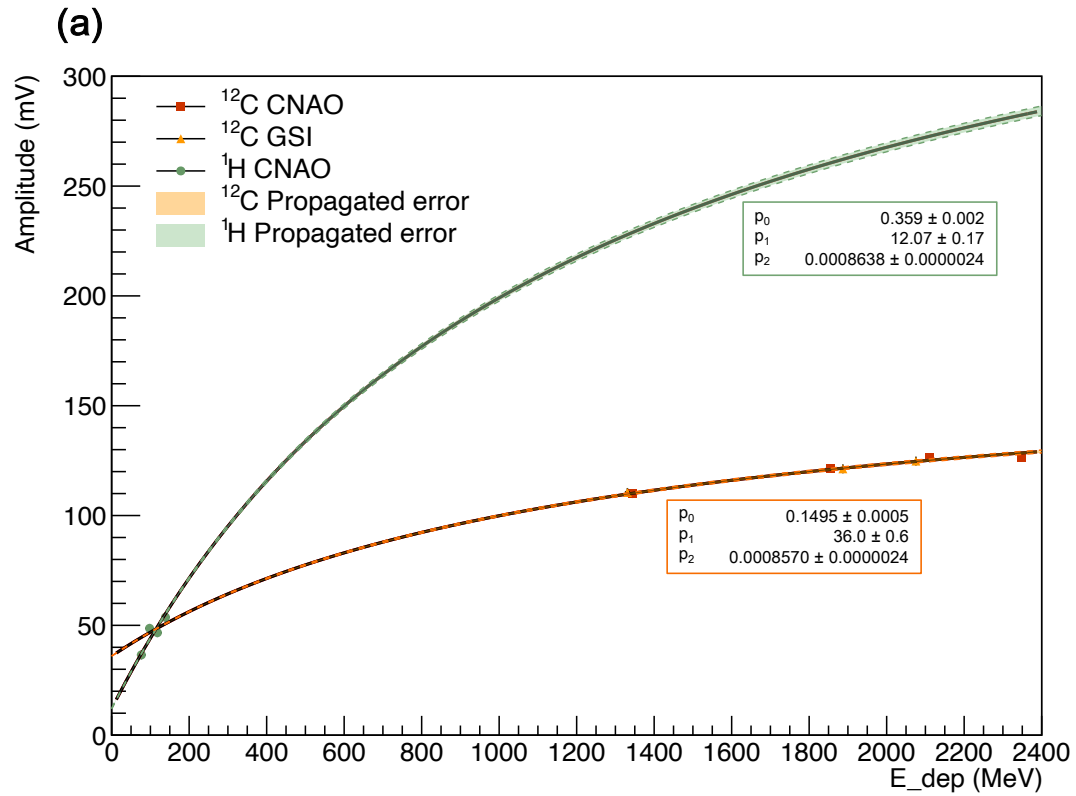


**Figure 5.** Calibration curves of the CeBr<sub>3</sub> crystal scintillator obtained with both protons and  $^{12}\text{C}$ , with an applied voltage of + 350 V for (a) and obtained with protons,  $^8\text{Li}$  and  $^{12}\text{C}$ , with an applied voltage of + 400 V for (b). Energies can be found on Table 1.

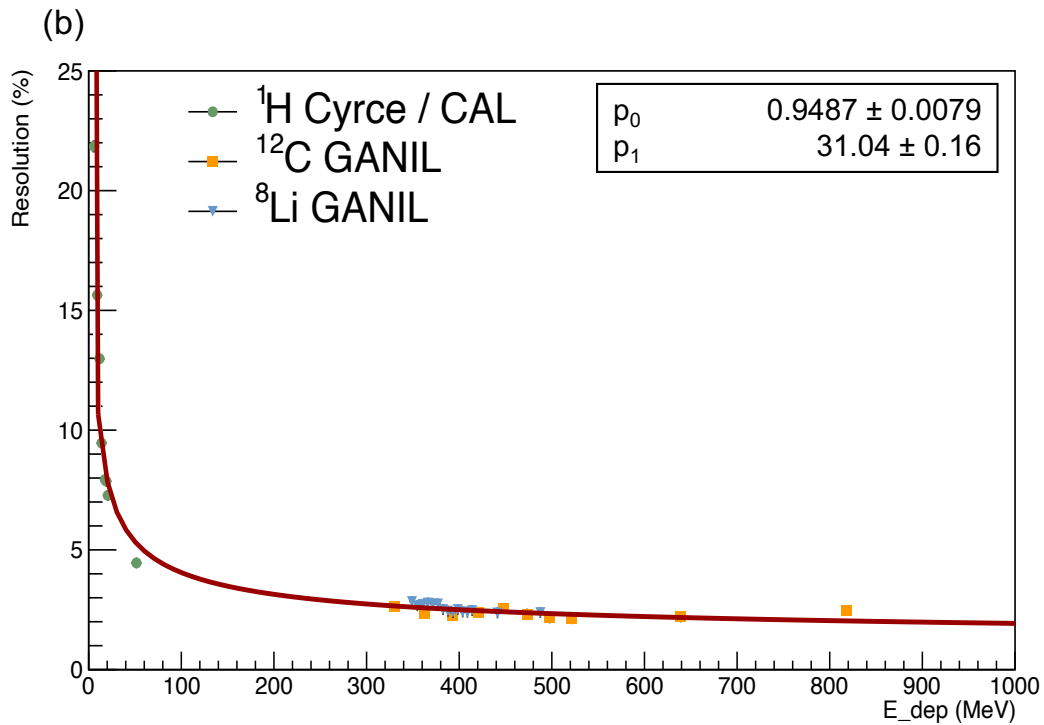
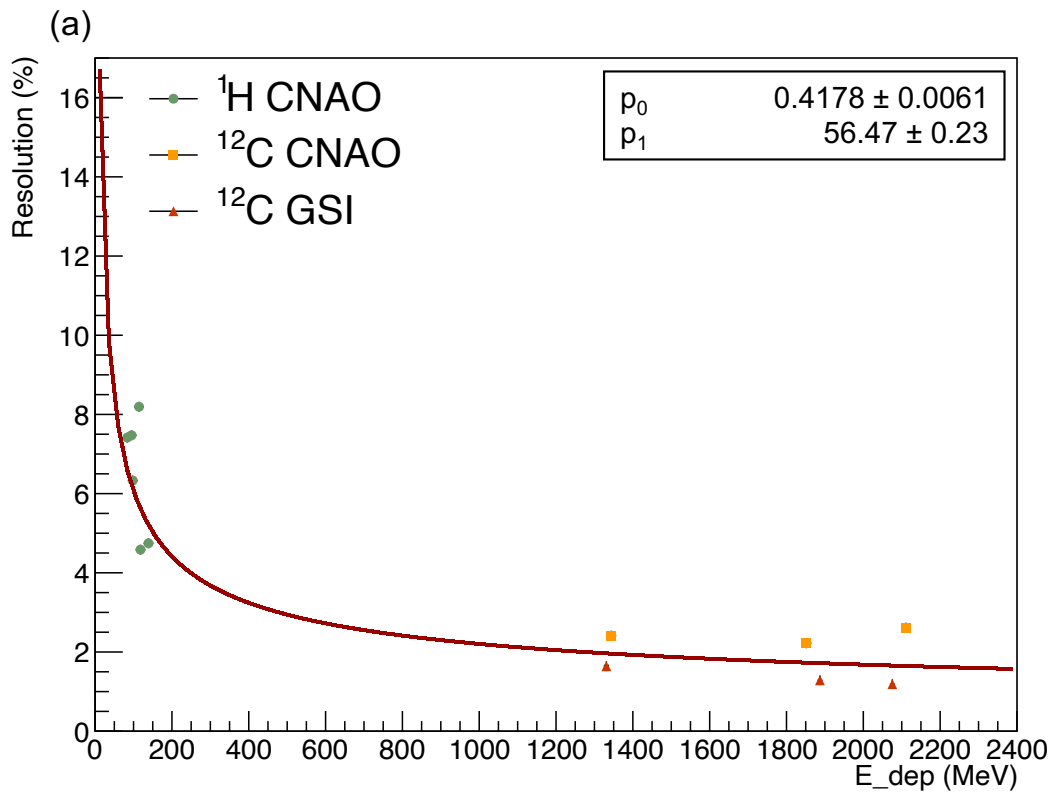


**Figure 6.** Resolution curves of the CeBr<sub>3</sub> crystal scintillator obtained with both protons and <sup>12</sup>C, with an applied voltage of + 350 V for (a) and obtained with protons, <sup>8</sup>Li and <sup>12</sup>C, with an applied voltage of + 400 V for (b). Energies can be found on Table 1.

MeV  $^1\text{H}$  beam represents a deviation of about 6%, which, while significant, remains manageable within the broader scope of experimental nuclear physics, where uncertainties can often span up to 10-20% depending on the complexity of the setup and the type of particles measured [15].

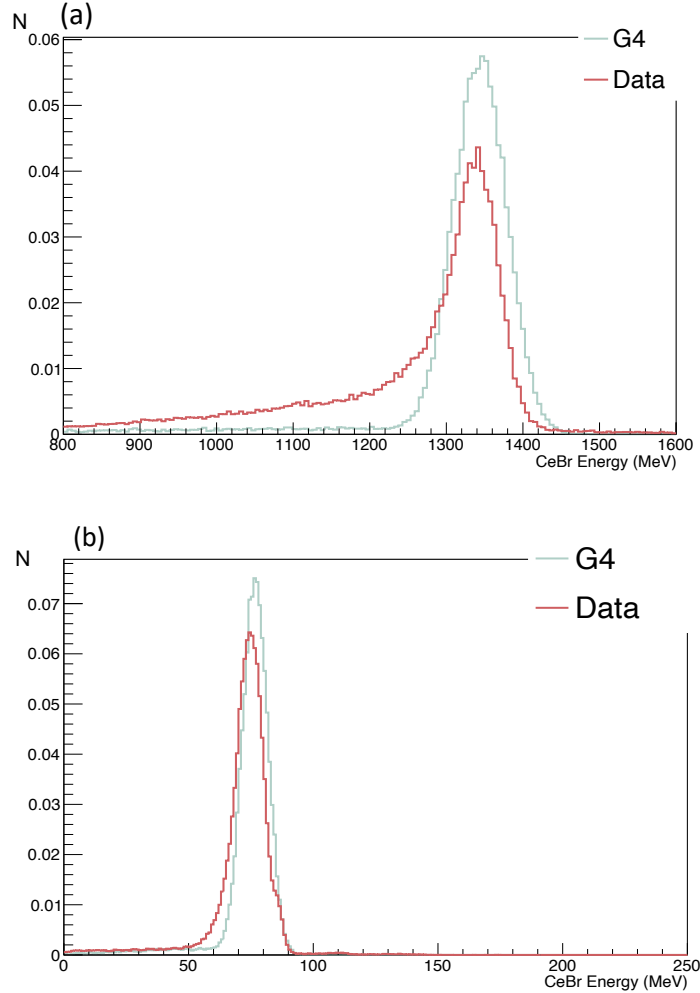


**Figure 7.**  $\text{CeBr}_3$  deposited energy comparison between G4 simulation and calibrated normalized data with a 120 MeV/u  $^{12}\text{C}$  beam (a) and a 100 MeV  $^1\text{H}$  beam.

### 3.3 Telescope ions identification

The identification of different ions using the  $\Delta E$ - $E$  telescope leverages the energy deposition characteristics in the plastic and  $\text{CeBr}_3$  scintillators. Figure 8 demonstrates the ability of the  $\Delta E$ - $E$  telescope to distinguish ions based on their charge state ( $Z$ ). The plot shows the energy deposited in the plastic scintillator ( $\Delta E$ ) as a function of the energy deposited in the  $\text{CeBr}_3$  scintillator ( $E$ ), for the secondary particles produced by a 200 MeV/u  $^{12}\text{C}$  ion beam on a RW3 target (tissue equivalent).

Each ion species ( $Z = 1$  to  $Z = 6$ ) forms a distinct branch in the  $\Delta E$ - $E$  space, reflecting its unique energy loss and remaining energy characteristics. The ability to resolve these branches accurately

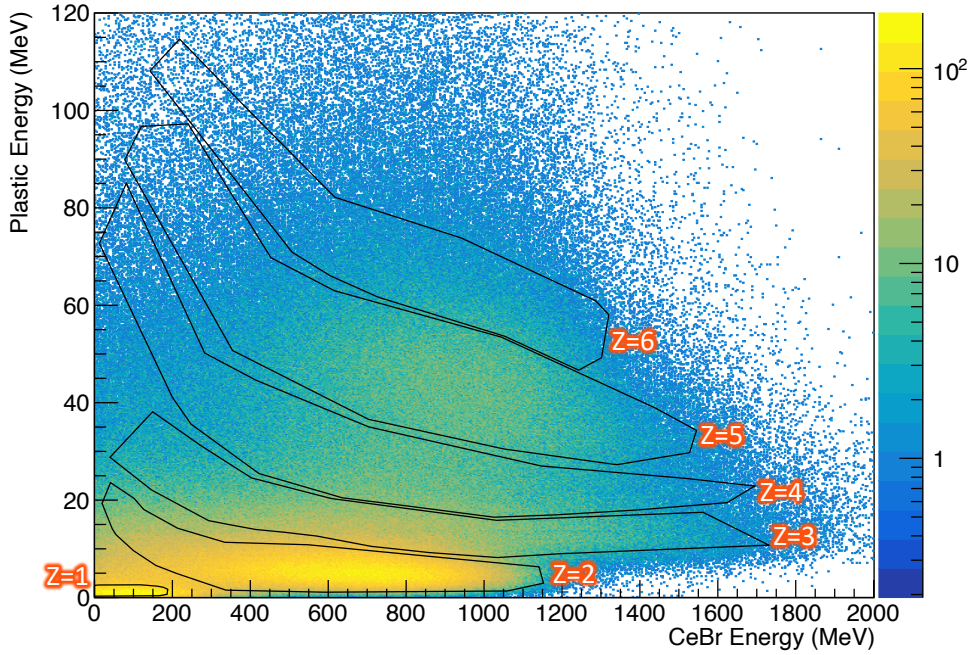


**Figure 8.** Energy deposited inside the plastic scintillator ( $\Delta E$ ) as a function of the energy deposited inside the  $\text{CeBr}_3$  ( $E$ ) for a  $^{12}\text{C}$  beam of 200 MeV/u on a 5 cm RW3 target and the detectors at  $5^\circ$  with the Z ions discrimination showed.

enables the identification of secondary charged particles generated during hadrontherapy scenario.

### 3.4 Time performance

A good time resolution ensures that the two measurements, energy loss and total energy, can be accurately correlated in time, aiding in precise particle identification. Moreover, this test is necessary as the telescope will also be used in  $\Delta E$ -ToF measurements for high-energy ions, as well as for detecting gammas and neutrons, necessitating rigorous temporal performance assessments. For instance, the FRACAS experiment achieved a time resolution of around 300 ps for similar high-energy ion beams [27]. These benchmarks illustrate the standards required for effective particle detection. The time resolution values were extracted from the experiments performed, with both protons and  $^{12}\text{C}$ . On Figure 9, the time discrepancies between the two detector are presented, for a 25 MeV protons beam (a) and a 180 MeV/u  $^{12}\text{C}$  beam (b).

The temporal resolution obtained from those distributions for the 180 MeV/u  $^{12}\text{C}$  beam, is of  $282 \pm 1$  ps. Similarly, for the plastic and  $\text{CeBr}_3$  detectors with 25 MeV protons beam, the time resolution was determined of  $171 \pm 1$  ps. The increase of the time resolution value for carbon ions is mainly due to the low voltage that was applied to the cerium bromide PMT (+ 350 V). These values represent crucial benchmarks in assessing the time performance of the detection system across varying beam energies and particle types. Such precise temporal resolution enables robust particle identification and TOF measurement, and enhances the overall capabilities of the experimental setup for the CLINM purpose.

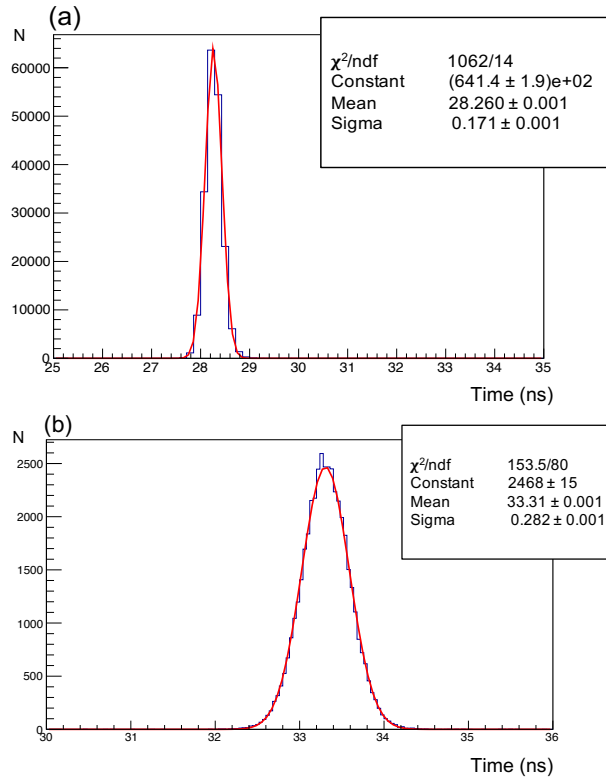


**Figure 9.** Resolution in time between the plastic with the  $\text{CeBr}_3$  and R7057 PMT with a 25MeV  $^1\text{H}$  beam (a) and XP3990 PMT with a 180 MeV/u  $^{12}\text{C}$  beam (b)

#### 4 Discussion

The calibration of the plastic scintillator yielded a calibration curve with two different PMTs both adhering to Birks' law, up to 50 MeV of deposited energy. This result demonstrates the reliability of the plastic scintillator's response to ion beams within this energy range. The energy resolution of the plastic scintillator was also examined, and it is noteworthy that the resolution improves as the deposited energy increases. This is consistent with the expected behavior, as higher energy ions generate more scintillation light, resulting in better energy resolution.

The  $\text{CeBr}_3$  crystal scintillator was calibrated with proton,  $^8\text{Li}$  and  $^{12}\text{C}$  ion beams. The calibration results show that the crystal scintillator follows the Birks' law up to 2350 MeV of deposited energy, which corresponds to the energy deposited by 200 MeV/u  $^{12}\text{C}$  ions (after traversing 2 mm of PMMA). This extended reliability is a valuable characteristic, as it allows for the accurate measurement of a wide range of ion energies encountered in hadrontherapy treatment (80 - 200 MeV/u for  $^1\text{H}$  beam and 120 - 400 MeV/u for  $^{12}\text{C}$  beam).

Furthermore, examination of calibration curves obtained with protons at different voltages, +350 V and +400 V exhibited consistency, indicative of the  $\text{CeBr}_3$  scintillator's efficient response to varied voltage settings for ion detection.

Notably, the Birks' law reflected a quenching effect of the scintillators, with an increase



in voltage corresponding to an increase in the Birks constant. This observation underscores the adaptability of the scintillator to diverse experimental conditions and provides options for optimizing its performance. The adherence to Birks' law across multiple ion types (protons,  $^8\text{Li}$ , and  $^{12}\text{C}$ ) and energy ranges (16 MeV to 2350 MeV deposited energy) is a notable result, as it ensures the system's reliability for clinical applications. This level of precision has not been demonstrated previously for  $\text{CeBr}_3$  scintillators in such conditions.

In addition to energy resolution, the time performance of our  $\Delta E$ -E telescope was also evaluated. Precise time measurements enable the correlation of energy loss and total energy, facilitating particle identification and background rejection. Unlike prior systems optimized for primary beam monitoring, this setup is uniquely calibrated for the detection of secondary charged particles, addressing a critical gap in data availability for hadrontherapy. The time resolution measurements exhibit a resolution of  $282 \pm 1$  ps for  $^{12}\text{C}$  ions of 180 MeV/u and  $171 \pm 1$  ps for 25 MeV protons. These results underscore the capability of this telescope to provide precise measurements in clinical conditions. The narrower time resolution for protons compared to  $^{12}\text{C}$  ions can be attributed to the differences in their masses and velocities. The timing resolution of 171–282 ps, coupled with an energy resolution on the order of 10 MeV, represents a substantial advancement in the detection of secondary particles. This precision enables not only better particle identification but also provides accurate input for Monte Carlo models, thereby improving the reliability of dose calculations.

The precise particle identification offered by the  $\Delta E$ -E telescope is critical for characterizing the secondary particles in clinical beams. Such measurements can improve our understanding of fragmentation processes in tissues and provide accurate inputs for Monte Carlo simulations, leading to more reliable treatment planning. The system's capability to detect ions across a wide range of charge states ensures its applicability in various clinical scenarios.

## 5 Conclusion

In the context of hadrontherapy, precision in measuring energy deposition stands as a fundamental requirement for optimizing treatment plans.

In this work, the calibration and performance evaluation of a  $\Delta E$ -E telescope was presented, designed for the detection of secondary charged particles generated in hadrontherapy under clinically relevant conditions. This telescope combines a thin plastic scintillator and a  $\text{CeBr}_3$  crystal scintillator, optimized for precision in energy and time measurements.

The calibration results demonstrate adherence to Birks' law, with the plastic scintillator effectively detecting energy deposition up to 50 MeV and up to 2350 MeV for the the  $\text{CeBr}_3$  crystal. These calibrations were achieved under multiple voltage settings and across a range of particle types (protons,  $^8\text{Li}$ ,  $^{12}\text{C}$ ), showcasing the versatility of the detection system.

The energy resolution was determined to be on the order of 10 MeV for both scintillators, ensuring precise identification of secondary particles. The system's time resolution was measured at  $282 \pm 1$  ps for 180 MeV/u  $^{12}\text{C}$  ions and  $171 \pm 1$  ps for 25 MeV protons. These results position the telescope as a robust tool for  $\Delta E$ -E and  $\Delta E$ -ToF measurements, capable of separating secondary particles generated during beam-tissue interactions.

In clinical terms, the telescope operates effectively within the energy ranges and ion types encountered in hadrontherapy. By accurately characterizing secondary charged particles, this study

addresses a critical gap in experimental data, providing valuable input for Monte Carlo simulations and improving treatment planning accuracy.

## Acknowledgments

Authors want to thank Claire-Anne Reidel and Christoph Schuy from the GSI biophysics department, whose help was crucial for carrying out this work. We also want to thank Angelica Facchetti from CNAO, Petter Hofverberg from CAL facility, and Michel Pelliccioli and Jacky Schuler from the Cyr c facility. Finally, this work would also not have been possible without the valuable help of C dric Mathieu and Thomas Adam. This work was possible thanks to the support of the HITRI+ project, the funding of the European Union’s Horizon 2020 Research and innovation (Grant Agreement N 101008548), and the ANR project funding ANR-23-CE31-0014.

## References

- [1] Cebr3 - cerium bromide scintillator crystal. *Advatech UK Ltd*.
- [2] Guide for physics lists. *Cancer*, Rev7.1(Release 11.1), April July 31st, 2023.
- [3] S. Agostinelli et al. Geant4—a simulation toolkit. *Nuclear Instruments and Methods in Physics Research Section A*, 506(3):250–303, 2003.
- [4] R. Anne and A.-C. Mueller. Lise 3: a magnetic spectrometer—wien filter combination for secondary radioactive beam production. *Nuclear Instruments and Methods in Physics Research Section B: Beam Interactions with Materials and Atoms*, 70:276, 1992.
- [5] J.B. Birks. Scintillations from organic crystals: Specific fluorescence and relative response to different radiations. *Proceedings of the Physical Society. Section A*, pages 64–874, 1951.
- [6] Dominique Breton, Eric Delagnes, Jihane Maalmi, and Pascal Rusquart. The wavecatcher family of sca-based 12-bit 3.2-gs/s fast digitizers. pages 1–8, 2014.
- [7] F. D. Brooks. Development of organic scintillators. *Nuclear Instruments and Methods*, 1979.
- [8] A. Bross, A. Pla-Dalmau, K. Mellott, and M. Knott. New developments in plastic scintillators. In *IEEE Nuclear Science Symposium Conference Record*, 2007.
- [9] T. T. B hlen et al. The fluka code: developments and challenges for high energy and medical applications. *Nuclear Data Sheets*, 120:211–214, 2014.
- [10] R. A. Cecil, B. D. Anderson, and R. Madey. Improved predictions of range-energy relations for heavy ions. *Nuclear Instruments and Methods*, 1979.
- [11] et al. Ch. Finck. Study for online range monitoring with the interaction vertex imaging method. *Physics in Medicine & Biology*, 62, 2017.
- [12] Julie Constanzo, Marie Vanstalle, Christian Finck, David Brasse, and Marc Rousseau. Dosimetry and characterization of a 25-MeV proton beam line for preclinical radiobiology research. *Medical Physics*, 46(5):2356–2362, May 2019.
- [13] M. Durante and J. S. Loeffler. Charged particles in radiation oncology. *Nature Reviews Clinical Oncology*, 7(1):37–43, 2010.

- [14] GSI Helmholtz Centre for Heavy Ion Research. Sis100/sis18 heavy ion synchrotron. [https://www.gsi.de/en/work/project\\_management\\_fair/sis100sis18\\_sis/heavy\\_ion\\_synchrotron\\_sis18](https://www.gsi.de/en/work/project_management_fair/sis100sis18_sis/heavy_ion_synchrotron_sis18).
- [15] R. Hamm and M. E. Hamm. *Industrial Accelerators and Their Applications*. 2012.
- [16] W. Hampel et al. Energy resolution of scintillation detectors at low light levels. *Nuclear Instruments and Methods in Physics Research Section A*, 299(1–3):308–312, 1990.
- [17] P. Hofverberg, M. Antunes, C. Armando, J.-M. Bergerot, E. Bourrel, J.-F. Dicarolo, G. Donadey, S. Dumas, D. Fayaud, J.-C. Grini, A. Giusto, Y. Payan, M. Rolion, C. Salicis, G. Angellier, J. Hérault, D. Maneval, M. Vidal, P. Mandrillon, F. Bezerra, J. Mekki, and R. Trimaud. A 60 MeV proton beam-line dedicated to research and development programs. *Applied Radiation and Isotopes*, 184:110190, June 2022.
- [18] G. Knoll. *Radiation Detection and Measurement*. John Wiley & Sons, 2010.
- [19] S. Kox et al. Trends of total reaction cross-sections for heavy ion collisions in the intermediate energy range. *Physical Review C*, 35(5):1678–1692, 1987.
- [20] W. R. Leo. *Techniques for Nuclear and Particle Physics Experiments: A How-To Approach*. Springer, 1994.
- [21] Alex Miller, Rachid Machrafi, and Abuzar Fariad. Investigation of the LaBr<sub>3</sub> scintillator response to heavy ions. *Radiation Measurements*, 115:43–48, August 2018.
- [22] H. Paganetti. *Proton therapy physics*. CRC Press, 2012.
- [23] Marco Pullia et al. The Experimental Beam Line at CNAO. In *7th International Particle Accelerator Conference*, page TUPMR038, 2016.
- [24] F.G.A. Quarati, Alan Owens, P. Dorenbos, J.T.M. de Haas, G. Benzoni, N. Blasi, C. Boiano, S. Brambilla, F. Camera, R. Alba, G. Bellia, C. Maiolino, D. Santonocito, M. Ahmed, N. Brown, S. Stave, H.R. Weller, and Y.K. Wu. High energy gamma-ray spectroscopy with LaBr<sub>3</sub> scintillation detectors. *Nuclear Instruments and Methods in Physics Research Section A: Accelerators, Spectrometers, Detectors and Associated Equipment*, 629(1):157–169, February 2011.
- [25] Benedetto Di Ruzza and The FOOT Collaboration. Fragmentation measurements in particle therapy: Status and plans of the foot experiment. *Journal of Physics: Conference Series*, 2374(1):012184, 2022.
- [26] S. Salvador et al. Timing capabilities of cebr<sub>3</sub> crystals for fast neutron detection. *Nuclear Instruments and Methods in Physics Research Section A*, 955:163309, 2020.
- [27] S. Salvador et al. Timing performances of a time-of-flight detection system for the fracas large acceptance mass spectrometer. *Journal of Instrumentation* 15, 2020.
- [28] D. Sarrut et al. A review of the use and applications of the geant4 monte carlo simulation toolkit in radiation therapy. *Frontiers in Oncology*, 4:365, 2014.
- [29] D. Schardt, T. Elsässer, and D. Schulz-Ertner. Heavy-ion tumor therapy: physical and radiobiological benefits. *Reviews of Modern Physics*, 82(1):383, 2010.